

Chemical tuning of samarium valence in mixed valence

 $(\text{Sm}_{1-x}\text{Ca}_x)_{2.75}\text{C}_{60}$ fullerides HPSTAR
1106-2021Naoya Yoshikane^a, Takeshi Nakagawa^b, Keisuke Matsui^a, Hitoshi Yamaoka^c,
Nozomu Hiraoka^d, Hirofumi Ishii^d, John Arvanitidis^{e, **}, Kosmas Prassides^{a, f, *}^a Department of Materials Science, Graduate School of Engineering, Osaka Prefecture University, Osaka 599-8531, Japan^b Center for High-Pressure Science & Technology Advanced Research, 100094 Beijing, PR China^c RIKEN SPring-8 Center, Sayo, Hyogo 679-5148, Japan^d National Synchrotron Radiation Research Center, Hsinchu 30076, Taiwan^e Physics Department, Aristotle University of Thessaloniki, 54124 Thessaloniki, Greece^f Advanced Institute for Materials Research (WPI-AIMR), Tohoku University, Sendai 980-8577, Japan

A B S T R A C T

Rare-earth (RE) fullerides are an intriguing family of materials in which electronic instabilities on the RE sublattice couple to the electronic and lattice degrees-of-freedom of the strongly-correlated fulleride sublattice. In particular, insulating $\text{Sm}_{2.75}\text{C}_{60}$ adopts an orthorhombic superstructure, arising from long-range ordering of Sm partial vacancies, and can be driven to a lattice-collapsed metallic state due to a valence transition towards Sm^{3+} upon pressurization. Here we use synchrotron X-ray absorption spectroscopy (XAS) at the Sm L_3 edge at ambient conditions to authenticate the mixed valence character of the material by identifying two features due to distinct Sm^{2+} and Sm^{3+} components – their relative intensity allows a direct measure of the average Sm valence in $\text{Sm}_{2.75}\text{C}_{60}$ at +2.07(3). We then attempt to mimic the physical pressure effect on the electronic properties by co-intercalation of the smaller-size valence-precise Ca^{2+} ion to form the series of ternary solid solutions, $(\text{Sm}_{1-x}\text{Ca}_x)_{2.75}\text{C}_{60}$ ($0 \leq x \leq 2/3$). XAS measurements in their high-resolution partial fluorescence yield (PFY) variance find that chemical pressure leads to an increase of the Sm^{3+} contribution to the average valence by >10% in the most contracted member, $(\text{Sm}_{1/3}\text{Ca}_{2/3})_{2.75}\text{C}_{60}$ of the present study with the average valence reaching a value of +2.33(2). Assuming full charge transfer between the metal ions and C_{60} , the charge on the C_{60} units remains invariant throughout at approximately -5.78 . This opens the possibility that the system can be tuned further towards the higher average valences needed for the high-pressure insulator-to-metal transition in $\text{Sm}_{2.75}\text{C}_{60}$ to be shifted to ambient pressure with a single-valence Sm^{3+} state accessible at a Ca content of $x \sim 0.9$.

1. Introduction

C_{60} fullerides –the metal intercalation compounds of C_{60} – are narrow band systems, which exhibit properties ranging from magnetism to high- T_c superconductivity and whose understanding poses considerable challenges due to the dominant role of electron correlations [1–3]. At the same time, the availability of different valence states such as $2+$ and $3+$ in selected RE metal ions (Sm, Eu, and Yb) [4], and the concomitant valence fluctuations of the $4f$ electrons, dominate the electronic response of these f -electron systems, leading to the emergence of mixed valence and exotic phenomena such as quantum criticality and unconventional superconductivity [5,6]. In these RE-based systems, there are two types of f electrons: localized core-like, determining the valence of the RE ions, and delocalized band-like f electrons that are formed through hybridization with the s - d bands participating in the bonding [4]. The latter are found in the trivalent RE-based systems, while their

localization favors a divalent ground state. The crossover between localized and itinerant f -electron states can be tuned by external stimuli, such as temperature, pressure, chemical substitution, and magnetic field [7]. Mixed valence phenomena in typical Kondo insulators and heavy fermions, such as the RE chalcogenides, borides and intermetallics, come into play when the $4f$ levels lie closely to the Fermi energy, while their electronic properties are entirely determined by the unconventional highly correlated character of the RE sublattice [8,9].

It is intriguing to combine the RE cation sublattice with the electronically active C_{60} anion sublattice, which may act as an electron reservoir accepting electrons from or donating electrons to the RE $4f/5d$ bands, thereby realizing a family of strongly correlated RE fullerides. Combining the electronically-active C_{60} anions with mixed configuration rare earths may lead to properties intrinsically unattainable in any other system currently available. Strong correlations will dominate the electronic properties of both the rare-earth cation and the C_{60} anion

* Corresponding author. Department of Materials Science, Graduate School of Engineering, Osaka Prefecture University, Osaka 599-8531, Japan.

** Corresponding author.

E-mail addresses: jarvan@physics.auth.gr (J. Arvanitidis), k.prassides@mtr.osakafu-u.ac.jp (K. Prassides).

sublattices allowing the emergence of unpredictable electronic properties such as Kondo phenomena of the f -electron sublattice co-existing with superconductivity supported by the C_{60} -based electrons. Indeed, similarly to typical Kondo insulators and heavy fermions, RE fullerides with stoichiometry $RE_{2.75}C_{60}$ (RE = Sm, Yb, Eu) display mixed valence phenomena and sensitivity of the RE valence to external stimuli, making them the first known molecular-based members of this fascinating class of materials [10]. One of the most spectacular findings in this research field was that, on cooling, the $Sm_{2.75}C_{60}$ fulleride exhibits an isosymmetric phase transition below 32 K, accompanied by a dramatic isotropic volume increase (negative thermal expansion, NTE) caused by a Sm valence transition from a mixed valence $(2 + \epsilon)^+$ state at room temperature towards $2+$ down to 2 K [11]. In addition, $Sm_{2.75}C_{60}$ undergoes a pressure-induced lattice collapse and changes in its optical properties at ~ 4 GPa, implying an insulator-to-metal transition due to an increase in Sm valence to higher values towards $3+$ [12,13]. This effect is analogous to the pressure-induced valence and the concomitant insulator-to-metal transitions encountered in mixed-valence Kondo insulators such as SmS or SmSe [14]. In particular, the huge NTE associated with the valency transition is recently drawing particular attention from the applications point of view in the family of materials with composition, $Sm_{1-x}R_xS$ (R = Y, Ce, Nd, etc) [15–17]. A valence fluctuation model between two nearly degenerate electronic configurations, $4f^65d^0$ and $4f^55d^1$, has been employed to describe the physics of these systems with the valence transition controlled by the Kondo temperature, reflecting the hybridization strength between the localized $4f$ and the conduction $5d$ electrons.

Here we report the results of ambient-temperature element-specific synchrotron XAS measurements of the average samarium valence in $Sm_{2.75}C_{60}$ to authenticate directly the mixed valence character of this material. In an attempt to mimic chemically the effect of external pressure application on the average Sm valence, we proceed to replace progressively the mixed valence $Sm^{(2+\epsilon)^+}$ ion by the smaller-in-size valence-precise alkaline earth Ca^{2+} ion to afford a series of ternary fullerides, $(Sm_{1-x}Ca_x)_{2.75}C_{60}$ ($0 \leq x \leq 2/3$). Synchrotron XAS measurements of the average Sm valence with increasing Ca^{2+} co-intercalant content, x reveal a monotonic increase with the parameter ϵ , which measures the Sm^{3+} contribution to the valence increasing by $>10\%$ across the present series.

2. Experimental

$(Sm_{1-x}Ca_x)_{2.75}C_{60}$ ($x = 0-1$) samples were prepared by direct reaction of stoichiometric quantities of C_{60} (super gold grade, $>99.9\%$), samarium (powder, Strem Chemicals, $>99.9\%$) and calcium (dendritic pieces, Sigma Aldrich, $>99.9\%$). Fine Ca powder was prepared by dissolving Ca pieces in dried liquid ammonia and then removing the ammonia by heating under vacuum. C_{60} , Sm and Ca powders were mechanically mixed, pressed into pellets and contained in a sealed tantalum cell inside an evacuated quartz tube at $550^\circ C$ for 3 days with one intermediate grinding. Rutherford backscattering spectrometry (RBS) was employed for a quantitative estimation of the metal content of the samples with nominal composition, $(Sm_{1-x}Ca_x)_{2.75}C_{60}$ ($x = 1/3, 2/3$), yielding Sm:Ca ratios of 2.04(11):1 and 0.49(1):1, respectively. High-resolution synchrotron X-ray powder diffraction (XRPD) experiments were carried out at ambient temperature on the ID31 beamline at the European Synchrotron Radiation Facility (ESRF), Grenoble, France. The samples were sealed in 0.5-mm diameter thin-wall glass capillaries and diffraction profiles were collected in continuous scanning mode at different wavelengths for different compositions ($x = 2/3$ sample at $\lambda = 0.41274 \text{ \AA}$; $x = 1/3$ sample at 0.85030 \AA). For the $x = 1/2$ sample, laboratory XRD data were collected with a Rigaku SmartLab (Mo $K\alpha$ radiation, $\lambda = 0.7093 \text{ \AA}$) diffractometer operating in transmission mode.

The X-ray absorption spectrum (XAS) of the parent system, $Sm_{2.75}C_{60}$ and the partial fluorescence yield-XAS (PFY-XAS) spectra of the ternary $(Sm_{1-x}Ca_x)_{2.75}C_{60}$ ($x = 1/3, 1/2, 2/3$) compounds at the Sm- L_3 edge were

recorded at the ID24 beamline (ESRF, France) and the Taiwan BL12XU beamline (SPring-8, Japan), respectively. PFY-XAS spectra were measured by fixing the emitted photon energy (*i.e.* by fixing the analyzer angle and the detector position) at $\sim 5636 \text{ eV}$ – around the maximum of the $L\alpha_1$ emission line – and scanning the incident photon energy across the Sm- L_3 edge [18]. This experimental method is able to count only the photons in the energy range of interest and dismiss other scattered photons or those due to fluorescence of other elements [19]. Since only one quantum transition (an intermediate state belonging to a shallow level) is selected, the lifetime broadening of the spectra that mainly comes from the deep core-hole in the final state, is suppressed, leading to significantly enhanced resolution compared to the conventional XAS technique [20–22].

3. Results and discussion

$Sm_{2.75}C_{60}$ crystallizes in the orthorhombic system (space group $Pcab$) with the Sm cations occupying off-centred tetrahedral and octahedral interstitial sites of the pristine face-centred cubic (fcc) C_{60} sublattice. One out of the eight tetrahedral sites is only partially occupied and the long range ordering of these sites results in a superstructure with all unit cell dimensions twice as large as those of the commonly encountered in fcc fulleride structures [11]. As an example of the studied series, the synchrotron XRPD profile of the $(Sm_{2/3}Ca_{1/3})_{2.75}C_{60}$ sample at room temperature is shown in Fig. 1. The analysis of the XRPD data was performed by means of the GSAS suite of Rietveld analysis programs, revealing that this ternary fulleride also adopts the same orthorhombic superstructure of $Sm_{2.75}C_{60}$ with structural parameters: $a = 28.09348$ (11) \AA , $b = 28.10186$ (11) \AA , $c = 28.08227$ (11) \AA and $V = 22170.4$ (3) \AA^3 (the weighted-profile and expected R-factors were $R_{wp} = 4.79\%$ and $R_{exp} = 2.53\%$, respectively) (Table S1). This is consistent with the recent finding that the other end member of the $(Sm_{1-x}Ca_x)_{2.75}C_{60}$ series, the pure alkaline-earth fulleride, $Ca_{2.75}C_{60}$, also adopts an identical structure [23].

Rietveld refinements of the XRPD data for the other $(Sm_{1-x}Ca_x)_{2.75}C_{60}$ compositions ($x = 1/2, 2/3$) confirmed the formation of the same orthorhombic superstructure across the series (Fig. S1 and S2, Tables S2 and S3) – the building block of the superstructure constituting $1/8$ of the unit cell is shown in the inset of Fig. 2. The extracted unit cell volumes of all members of the series obey Vegard's law and are displayed in Fig. 2. It is apparent that there is a quasilinear volume decrease with increasing Ca content, x , thus confirming the formation of a solid solution for the mixed compounds and implying that the metal cations are randomly distributed in the available tetrahedral and octahedral lattice sites [24]. Attempts to search for preferential occupation of the smaller tetrahedral interstices by the smaller Ca^{2+} ions in the course of the Rietveld refinements of the diffraction profiles provided no evidence for such a tendency. The gradual unit cell volume decrease with increasing Ca content across the series reflects the difference in ionic radius between the metal cations – Ca^{2+} (0.99 \AA) is considerably smaller than Sm^{2+} (1.14 \AA) and only marginally larger than Sm^{3+} (0.96 \AA) [25]. This is further enhanced by the accompanying increase in average Sm valence with increasing Ca content (*vide infra*).

The valence states of the Sm ions in the $(Sm_{1-x}Ca_x)_{2.75}C_{60}$ ($x = 0, 1/3, 1/2, 2/3$) fullerides at ambient conditions can be directly extracted by using element-specific, bulk-sensitive spectroscopic techniques such as XAS at the Sm- L_3 absorption edge. The corresponding XAS spectrum of $Sm_{2.75}C_{60}$ and PFY-XAS spectra of the $(Sm_{1-x}Ca_x)_{2.75}C_{60}$ ($x = 1/3, 1/2, 2/3$) compositions are presented in Fig. 3(a). As expected, the resolution of the latter spectra is significantly improved due to the suppression of the lifetime broadening. For a particular valence state of the Sm ions in a Sm-based system, a strong white line is observed at the edge because of the high density of dipole-allowed $5d$ states above the Fermi level [26]. Moreover, the thresholds associated with the Sm^{2+} and Sm^{3+} ions are separated by $\sim 7 \text{ eV}$ due to the final-state interaction between the core hole and the $4f$ shell, allowing the observation of a mixed valence

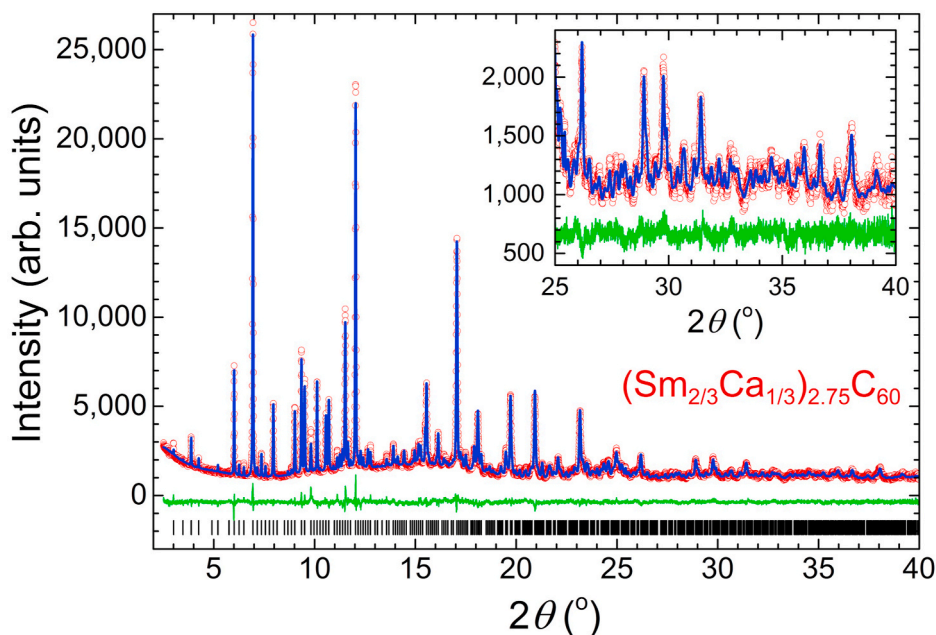


Fig. 1. Final observed (red circles) and calculated (blue solid line) synchrotron X-ray ($\lambda = 0.85030 \text{ \AA}$) powder diffraction profiles of the $(\text{Sm}_{2/3}\text{Ca}_{1/3})_{2.75}\text{C}_{60}$ sample at ambient conditions. The lower green solid line shows the difference profile and the tick marks show the reflection positions. The *inset* shows an expanded view of the quality of the fit at high Bragg angles.

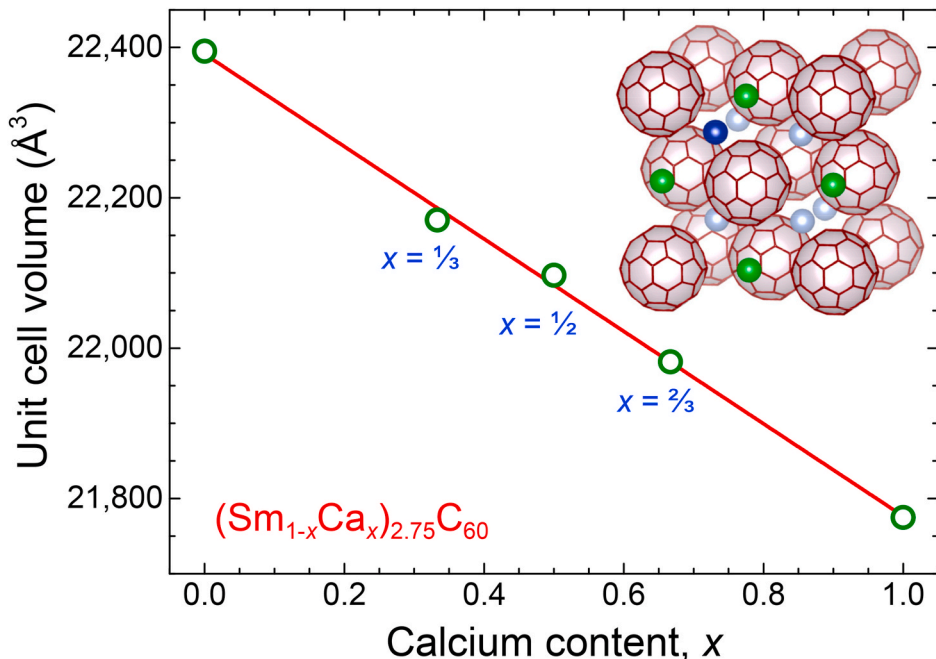


Fig. 2. Unit cell volume vs calcium content, x for the $(\text{Sm}_{1-x}\text{Ca}_x)_{2.75}\text{C}_{60}$ ($x = 0-1$) fullerides. The *inset* shows the building block of the unit cell of the orthorhombic superstructure of these compounds, formed by doubling the subcell along the three lattice directions. Green and light-grey spheres correspond to off-centred octahedral and tetrahedral metal cations, respectively, while the dark-blue sphere represents the partially occupied tetrahedral site.

ground state in the system and the quantitative evaluation of the average valence [27]. From Fig. 3(a), it is evident that in all the studied compounds we observe two main peaks, corresponding to the $2p \rightarrow 5d$ dipolar excitations for divalent and trivalent Sm states, superimposed on a background originating from transitions to the continuum. The appearance of the two peaks unambiguously evidences the mixed valence state of the Sm ions in all the Sm-based fullerides, while the higher intensity of the Sm^{2+} peak compared to that of the Sm^{3+} peak qualitatively implies that the average valence is closer to $2+$ rather than

to $3+$. At the same time, the intensity of the higher energy peak attributed to trivalent Sm increases at the expense of the peak attributed to the divalent Sm state with increasing calcium content, implying a gradual increase of the average Sm valence towards higher values approaching $3+$ with increasing Ca content, x .

In order to extract the average valence of the Sm ions in the $(\text{Sm}_{1-x}\text{Ca}_x)_{2.75}\text{C}_{60}$ compounds, the data were fitted by appropriate functions to account for the white lines and the background. As an example, the fit of the PFY-XAS spectrum of $(\text{Sm}_{2/3}\text{Ca}_{1/3})_{2.75}\text{C}_{60}$ together with the individual

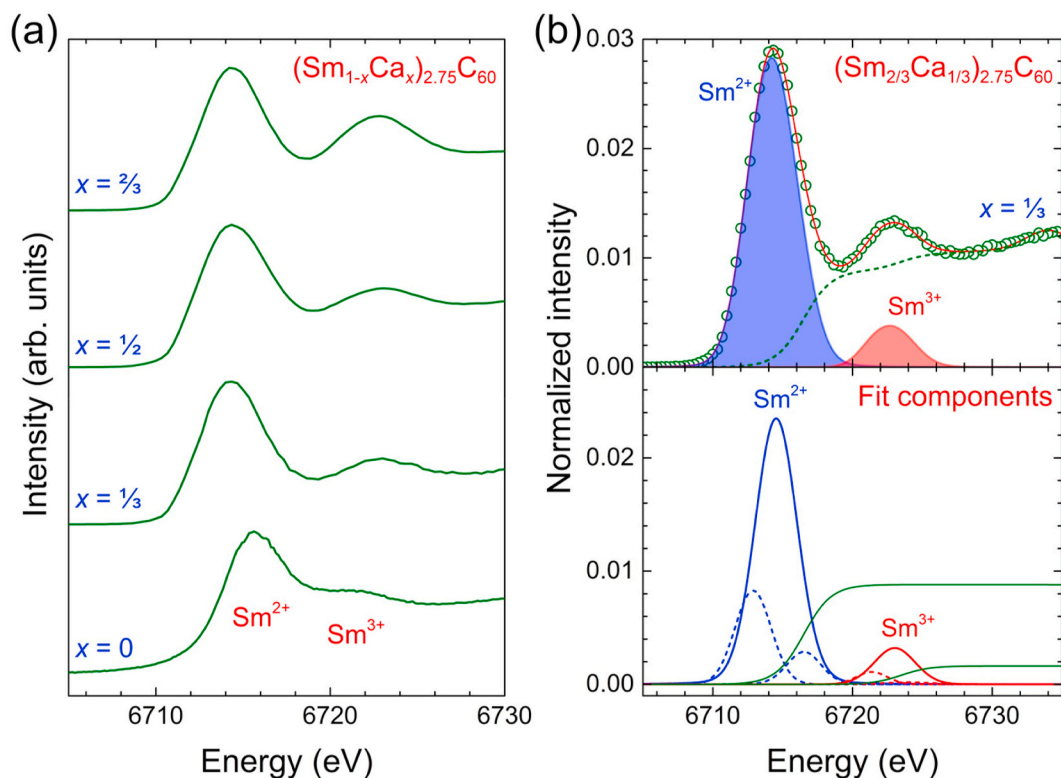


Fig. 3. (a) TFY-XAS spectrum of $\text{Sm}_{2.75}\text{C}_{60}$ and PFY-XAS spectra of the $(\text{Sm}_{1-x}\text{Ca}_x)_{2.75}\text{C}_{60}$ ($x = 1/3, 1/2, 2/3$) compounds at the Sm- L_3 edge, recorded at ambient conditions. (b) **Top panel:** representative fit (solid line through the data) of the experimental data (open circles) for $(\text{Sm}_{2/3}\text{Ca}_{1/3})_{2.75}\text{C}_{60}$, illustrating the two main peaks, as shaded areas, corresponding to the $2p \rightarrow 5d$ dipolar excitations for Sm^{2+} (purple) and Sm^{3+} (red) Sm states and the background accounting for the transitions to the continuum (dotted line). **Bottom panel:** fit components employed in the fitting procedure of the experimental data for all compounds. Each of the two peaks was fitted by three Voigt functions, while two arctangent functions were used to fit the background.

fitting functions employed are illustrated in Fig. 3(b). Since the continuum part enhances the uncertainty, we only considered the white line region to estimate the respective intensity of each component attributed to a particular valence state of Sm. Each component was fitted by the

sum of an arctangent continuum excitation background and three Voigt functions (one main and two satellites) to satisfactorily reproduce the white peaks. Electronic structure calculations and comparison of the density-of-states obtained for the Sm 5d band and the crystal-field split

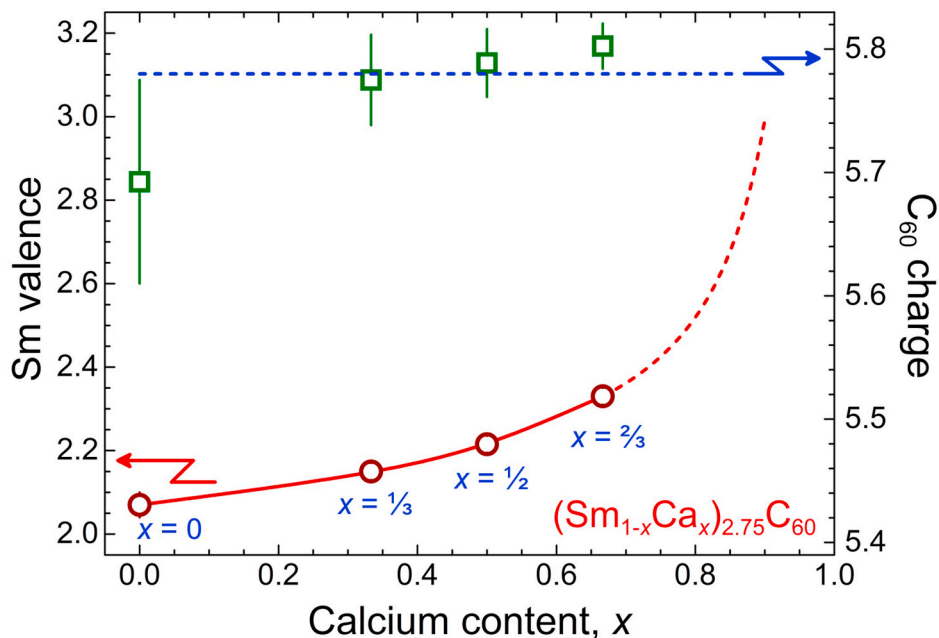


Fig. 4. Extracted Sm valence (open circles – left scale) and estimated C_{60} charge (open squares – right scale) vs calcium content, x for the $(\text{Sm}_{1-x}\text{Ca}_x)_{2.75}\text{C}_{60}$ series. The solid red line through the Sm valence data is a guide the eye with the dashed red line marking extrapolation of the data towards a value of 3+ assuming a fixed C_{60} charge across the series. The dashed blue line is drawn at the average C_{60} charge of 5.78.

t_{2g} and e_g subbands with the experimental PFY-XAS data for Sm and Yb monochalcogenides allowed for the assignment of the three components constituting the divalent white peak [28]. Namely, the low and the high energy satellite components – dashed lines in the bottom panel of Fig. 3 (b) – are of pure t_{2g} and e_g character, while the main central component (solid line) has mixed character.

The average Sm valence is derived from the relative intensity of the divalent and trivalent peaks with the simple formula: $\nu = 2 + I(3+)/[I(2+) + I(3+)]$ [29], where $I(2+)$ and $I(3+)$ are the integrated intensities of the white XAS peaks attributed to Sm^{2+} and Sm^{3+} , respectively (corresponding shaded areas in Fig. 3(b) – top panel). From the fit components illustrated in Fig. 3(b), we extract an average valence state of Sm for $x = 1/3$ of 2.15(2). This value is in fair agreement with an earlier resonant inelastic X-ray scattering (RIXS) study of $(\text{Sm}_{2/3}\text{Ca}_{1/3})_{2.75}\text{C}_{60}$ [10], confirming thus the reliability and reproducibility of the Sm valence estimations in these systems by different spectroscopic techniques. The derived average valence of the Sm ions in the studied $(\text{Sm}_{1-x}\text{Ca}_x)_{2.75}\text{C}_{60}$ compounds is depicted in Fig. 4. It is found that it increases monotonically at an accelerating rate with increasing divalent calcium content from 2.07(3)+ for $x = 0$ to +2.21(2) for $x = 1/2$ to +2.33(2) for $x = 2/3$, revealing that the Sm valence can be controlled here chemically by the co-intercalation of the valence-precise Ca^{2+} ion. This is reminiscent of the situation encountered in Sm monochalcogenides upon chemical substitution by divalent and trivalent ions [30,31] – in which size and electronic structure effects have been shown to control valence fluctuations – thereby strengthening the commonalities between the distinct mixed valence Sm-based systems.

Assuming complete electron transfer from the metal ions to the molecular cages, although the situation should be more complicated particularly due to the strong Sm– C_{60} orbital hybridization [13], we can roughly estimate the charge on the C_{60} units and the filling of the C_{60} t_{1u} -derived band in the $(\text{Sm}_{1-x}\text{Ca}_x)_{2.75}\text{C}_{60}$ fullerides. Remarkably it appears that the C_{60} charge remains essentially invariant across the series pinned to a value approximately equal to -5.78 (dashed horizontal line in Fig. 4). Therefore, the nearly composition-independent filling level of the t_{1u} band of C_{60} together with the robust divalent state of the Ca^{2+} ions act as fine chemical tuning parameters of the mixed valence state of the Sm ions. Assuming that this trend will persist to compositions with higher Ca content level ($x > 2/3$) than those accessed in this study, we conjecture that this provides the opportunity to access the higher average Sm valences achieved by pressurization and needed to drive the system metallic at ambient pressure. Eventually, complete suppression the Sm mixed valence and a transition to a trivalent Sm electronic state should occur in the vicinity of $x \sim 0.9$, i.e. for a fulleride composition, $(\text{Sm}_{0.1}\text{Ca}_{0.9})_{2.75}\text{C}_{60}$ (dashed red line in Fig. 4).

4. Conclusion

In conclusion, we have presented synchrotron XAS measurements on the series of ternary alkaline earth/rare earth metal $(\text{Sm}_{1-x}\text{Ca}_x)_{2.75}\text{C}_{60}$ ($0 \leq x \leq 2/3$) fullerides. Structural characterization by high-resolution synchrotron X-ray powder diffraction reveals that Vegard's law is obeyed and the mixed Sm/Ca compounds form nearly ideal solid solutions. The mixed valence state of Sm in all the members of this family was authenticated by XAS in both its variants, total and partial fluorescence yield (TFY-XAS and PFY-XAS). In particular, it emerges that the robust +2 charge state of the smaller-size alkaline earth co-dopant together with a nearly invariant charge state of the C_{60} units at -5.78 combine to allow continuous chemical tuning of the mixed valence of the Sm ions in a very precise fashion – the average oxidation state increases monotonically and rapidly with increasing Ca content, x towards a putative transition to a single valent Sm^{3+} state at $x \sim 0.9$. Chemical pressure thus turns out to be an efficient stimulus towards achieving the high average Sm valences away from +2 needed to drive the material metallic, thereby shifting the physical pressure-induced insulator-to-metal transition to ambient conditions. Recently a paper appeared

reporting the evolution of the Sm valence with applied pressure in one of the members of this family of materials [32].

CRedit authorship contribution statement

Naoya Yoshikane: participation in experiment, data analysis. **Takeshi Nakagawa:** synthesis, data analysis. **Keisuke Matsui:** participation in experiment, data analysis. **Hitoshi Yamaoka:** experimental support, data analysis. **Nozomu Hiraoka:** experimental support. **Hirofumi Ishii:** experimental support. **John Arvanitidis:** participation in experiment, data analysis, Writing - original draft. **Kosmas Prassides:** Conceptualization, data analysis, Writing - original draft.

Declaration of competing interest

The authors declare that they have no known competing financial interests or personal relationships that could have appeared to influence the work reported in this paper.

Acknowledgements

We thank the ESRF and SPring-8 for the provision of beamtime and Dr. D. Christofilos, Dr. S. M. Souliou, and Dr. V. Cuartero for their contribution during the measurement of the XAS spectrum of $\text{Sm}_{2.75}\text{C}_{60}$ at the ESRF. This work was financially supported by Grants-in-Aid for Scientific Research (JSPS KAKENHI Grant Numbers JP18H04303, JP18K18724, and JP19H04590) by the Ministry of Education, Culture, Sports, Science and Technology (MEXT), Japan, by the Murata Foundation, and by the KAKENHI Specific Support Operation of Osaka Prefecture University. The experiments at the SPring-8 Taiwan beamline BL12XU were performed under SPring-8 Proposal No. 2017B4268 and 2018B4252, corresponding to NSRRC Proposal No. 2018-1-058-1 and 2018-1-058-3, respectively.

Appendix A. Supplementary data

Supplementary data to this article can be found online at <https://doi.org/10.1016/j.jpcs.2020.109822>.

References

- [1] (a) J.E. Han, O. Gunnarsson, V.H. Crespi, *Phys. Rev. Lett.* 90 (2003) 167006; (b) M. Capone, M. Fabrizio, C. Castellani, E. Tosatti, *Rev. Mod. Phys.* 81 (2009) 943; (c) Y. Nomura, S. Sakai, M. Capone, R. Arita, *Sci. Adv.* 1 (2015), e1500568.
- [2] (a) Y. Takabayashi, A.Y. Ganin, P. Jeglic, D. Arcon, T. Takano, Y. Iwasa, Y. Ohishi, M. Takata, N. Takeshita, K. Prassides, M.J. Rosseinsky, *Science* 323 (2009) 1585; (b) A.Y. Ganin, Y. Takabayashi, P. Jeglic, D. Arcon, A. Potocnik, P.J. Baker, Y. Ohishi, M.T. McDonald, M.D. Tzirakis, A. McLennan, G.R. Darling, M. Takata, M. J. Rosseinsky, K. Prassides, *Nature* 466 (2010) 221; (c) Y. Ihara, H. Alloul, P. Wzietek, D. Pontiroli, M. Mazzani, M. Ricco, *Phys. Rev. Lett.* 104 (2010) 256402; (d) R.H. Zadik, Y. Takabayashi, G. Klupp, R.H. Colman, A.Y. Ganin, A. Potocnik, P. Jeglic, D. Arcon, P. Matus, K. Kamaras, Y. Kasahara, Y. Iwasa, A.N. Fitch, Y. Ohishi, G. Garbarino, K. Kato, M.J. Rosseinsky, K. Prassides, *Sci. Adv.* 1 (2015), e1500059.
- [3] (a) Y. Takabayashi, K. Prassides, *Struct. Bond* 172 (2016) 119; (b) Y. Takabayashi, K. Prassides, *Phil. Trans. R. Soc. A* 374 (2016) 20150320; (c) Y. Kasahara, Y. Takeuchi, R.H. Zadik, Y. Takabayashi, R.H. Colman, R. D. McDonald, M.J. Rosseinsky, K. Prassides, Y. Iwasa, *Nat. Commun.* 8 (2017) 14467; (d) H.E. Okur, K. Prassides, *J. Phys. Chem. Solid.* 131 (2019) 44.
- [4] P. Strange, A. Svane, W.M. Temmerman, Z. Szotek, H. Winter, *Nature* 399 (1999) 756.
- [5] G.R. Stewart, *Rev. Mod. Phys.* 73 (2001) 797.
- [6] H.Q. Yuan, F.M. Grosche, M. Deppe, C. Geibel, G. Sparn, F. Steglich, *Science* 302 (2003) 2104.
- [7] C.M. Varma, *Mixed valence compounds*, *Rev. Mod. Phys.* 48 (1976) 219.
- [8] P. Wachter, K.A. Gschneidner, L. Eyring, G.H. Lander, in: G.R. Chopin (Ed.), *Handbook on the Physics and Chemistry of Rare Earths*, vol. 19, Elsevier Science B. V., Amsterdam, 1994, pp. 177–382.
- [9] D. Malterre, M. Griioni, Y. Baer, *Adv. Phys.* 45 (1996) 299.
- [10] K. Prassides, Y. Takabayashi, T. Nakagawa, *Phil. Trans. R. Soc. A* 366 (2008) 151.

- [11] J. Arvanitidis, K. Papagelis, S. Margadonna, K. Prassides, A.N. Fitch, *Nature* 425 (2003) 599.
- [12] J. Arvanitidis, K. Papagelis, S. Margadonna, K. Prassides, *Dalton Trans.* (2004) 3144.
- [13] S.M. Souliou, J. Arvanitidis, D. Christofilos, K. Papagelis, S. Ves, G.A. Kourouklis, K. Prassides, Y. Iwasa, K. Syassen, *High Pres. Res.* 31 (2011) 13.
- [14] A. Jayaraman, V. Narayanamurti, E. Bucher, R.G. Maines, *Phys. Rev. Lett.* 25 (1970) 1430.
- [15] K. Takenaka, *Front. Chem.* 6 (2018) 267.
- [16] Y. Yokoyama, H. Hasegawa, Y. Mizuno, D. Asai, Y. Okamoto, H.S. Suzuki, K. Takehana, Y. Imanaka, K. Takenaka, *Phys. Rev. B* 100 (2019) 245143.
- [17] D.G. Mazzone, M. Dzero, A.M. M. Abeykoon, H. Yamaoka, H. Ishii, N. Hiraoka, J.-P. Rueff, J. M. Ablett, K. Imura, H. S. Suzuki, J. N. Hancock, I. Jarrige, *Phys. Rev. Lett.* 124 (2020) 125701.
- [18] H. Yamaoka, I. Jarrige, N. Tsujii, M. Imai, J.-F. Lin, M. Matsunami, R. Eguchi, M. Arita, K. Shimada, H. Namatame, M. Taniguchi, M. Taguchi, Y. Senba, H. Ohashi, N. Hiraoka, H. Ishii, K.-D. Tsuei, *Phys. Rev. B* 83 (2011) 104525.
- [19] P. Glatzel, R. Alonso-Mori, D. Sokaras, in: J.A. van Bokhoven, C. Lamberti (Eds.), *X-ray Absorption and X-Ray Emission Spectroscopy: Theory and Applications*, John Wiley & Sons Ltd, Chichester, 2016, pp. 125–153.
- [20] C. Dallera, M. Grioni, A. Shukla, G. Vankó, J.L. Sarrao, J.P. Rueff, D.L. Cox, *Phys. Rev. Lett.* 88 (2002) 196403.
- [21] J.-P. Rueff, A. Shukla, *Rev. Mod. Phys.* 82 (2010) 847.
- [22] H. Yamaoka, *High Pres. Res.* 36 (2016) 262.
- [23] A.G.V. Terzidou, T. Nakagawa, N. Yoshikane, R. Rountou, J. Rix, O. Karabinaki, D. Christofilos, J. Arvanitidis, K. Prassides, *Mod. Phys. Lett. B* 34 (2020) 2040056.
- [24] K.T. Jacob, S. Raj, L. Rannesh, *Int. J. Mat. Res.* 98 (2007) 776.
- [25] R.D. Shannon, *Acta Crystallogr. A* 32 (1976) 751.
- [26] G. Materlik, J.E. Muller, J.W. Wilkins, *Phys. Rev. Lett.* 50 (1983) 267.
- [27] E. Beaurepaire, J.P. Kappler, G. Krill, *Phys. Rev. B* 41 (1990) 6768.
- [28] I. Jarrige, H. Yamaoka, J.-P. Rueff, J.-F. Lin, M. Taguchi, N. Hiraoka, H. Ishii, K. D. Tsuei, K. Imura, T. Matsumura, A. Ochiai, H.S. Suzuki, A. Kotani, *Phys. Rev. B* 87 (2013) 115107.
- [29] H. Yamaoka, N. Tsujii, M.-T. Suzuki, Y. Yamamoto, I. Jarrige, H. Sato, J.-F. Lin, T. Mito, J. Mizuki, H. Sakurai, O. Sakai, N. Hiraoka, H. Ishii, K.-D. Tsuei, M. Giovannini, E. Bauer, *Sci. Rep.* 7 (2017) 5846.
- [30] A. Jayaraman, P. Dernier, L.D. Longinotti, *Phys. Rev. B* 11 (1975) 2783.
- [31] A. Jayaraman, R.G. Maines, *Phys. Rev. B* 19 (1979) 4154.
- [32] N. Yoshikane, K. Matsui, T. Nakagawa, A.G.V. Terzidou, Y. Takabayashi, H. Yamaoka, N. Hiraoka, H. Ishii, J. Arvanitidis, K. Prassides, Pressure-induced valence transition in the mixed-valence $(\text{Sm}_{1/3}\text{Ca}_{2/3})_{2.75}\text{C}_{60}$ fulleride, *Mater. Chem. Front.* (2020), <https://doi.org/10.1039/DOQM00707B>.